On the barotropic planetary oscillations of the Pacific

by Arthur J. Miller[1]

ABSTRACT
Free linear solutions of the barotropic shallow-water equations are computed for a variety of basin shapes and topographies relevant to the Pacific Ocean. Attention is drawn to the 2-day to 6-day period band within which large-scale coherency is observed in Pacific tide-gauge records of sea level. In a particular model basin with realistic topography, the fundamental planetary mode of the Pacific occurs with a period of 3 days and four other planetary-topographic modes populate the 4–6 day period band. We argue that the frequencies and structures of these modes are representative of the largest-scale vorticity oscillations of the Pacific and may help account for the observed broad-bandedness of sea-level in the 4–6 day period band. These predictions will guide future analyses of sea-level and bottom-pressure observations from which a direct estimate of the frictional damping of barotropic Rossby waves may ultimately be obtained.

1. Introduction

The planetary (or Rossby) normal modes of linear, barotropic, flat-bottomed ocean models were calculated, for various idealized geometries, by Longuet-Higgins (1964; 1965; 1966), Rattray and Charnell (1966), Longuet-Higgins and Pond (1970), Mofjeld and Rattray (1971) and Christensen (1973) as models for the planetary oscillations of the real oceans. Questions have arisen concerning the relevance of the flat-bottom assumption because of the many subsequent studies (e.g., Rhines and Bretherton, 1973; Anderson and Killworth, 1977; Ripa, 1978) of the strong, and perhaps dominating, effects of smaller-scale topography on the planetary waves. Indeed, the vorticity modes which occurred in the spectrum of shallow-water normal modes computed by Platzman *et al.* (1981), hereinafter PCHS81, for the world ocean with topography, all appeared to be controlled by topographic gradients. It remains unclear whether basin-scale vorticity modes which are significantly controlled by the planetary vorticity gradient can exist in the presence of real ocean topography.

In spite of the preceding remarks, a remarkable signal appears in observations of sea level from tide-gauge stations in the Pacific. Luther (1982) has shown the existence of a dynamic (nonisostatic) component of oceanic response to large-scale atmospheric-pressure forcing. The westward-propagating response is coherent over basin scales in a broad (4–6 day) period band, which suggests the presence of basin mode which is

1. Scripps Institution of Oceanography and California Space Institute, University of California, San Diego, California, 92093, U.S.A.

heavily damped. Indeed, Luther (1982), under the assumption that a single mode caused the 4–6 day peak, estimated an amplitude e-folding time of 6 days based on the width of the power-spectral peak. However, if more than one mode contributes to the peak the damping may be weaker. Miller (1986a) suggested that, even if a single flat-bottom mode is predicted to occur in the 4–6 day band, multiple occurrences (rending) of the open-ocean structure of a single mode could arise due to an interaction with topographic waves associated with continental shelf-slopes or distant ridges.

Luther's (1982) observations provide a unique opportunity to obtain a direct estimate of the frictional damping of Rossby waves. For this goal to be achieved, it is imperative to predict the number and structure of planetary modes which occur in the 4–6 day period band. The computations reported herein comprise the first systematic attempt to determine the largest-scale vorticity modes of the Pacific Ocean for periods as long as 6 days. Since the supercomputers of this era are yet inadequate to include the scale separation necessary to properly resolve realistic relief over basin scales, physical assumptions must complement direct numerical calculation. Therefore, based on the results of computing quasigeostrophic normal modes in idealized rigid-lid ocean basins with well-resolved topography (Miller, 1986a, b), we contend that the dominant effects of small-scale (unresolved) topography on large-scale vorticity waves are as follows:

i. Gentle bottom roughness, for which the resonant periods of topographic waves are much longer than the periods of the planetary waves, alters the Rossby modes in a manner which may be rationalized by second-order perturbation theory. Structural changes appear as weak topographic-scale perturbations while frequency shifts are toward higher frequencies.

ii. Large-scale planetary waves can propagate intact over strong, small-scale, isolated features such as seamounts (see Fig. 1). Perturbations to frequency may be of either sign.

iii Topographic features, such as continental shelf-slopes and mid-ocean ridges, which support topographic waves with resonant period comparable to the planetary waves can rend a nondegenerate basin-wide planetary mode into a family of basin-wide modes of slightly-differing frequencies and differing structures near the topography, but with nearly identical structure away from the topography.

We emphasize that real ocean topography can include stronger roughness, nonisolated seamounts, and steeper shelf-slopes than supposed, respectively, in (i), (ii), and (iii). Understanding the effects of realistic, large-amplitude, small-scale, irregular bathymetry on large-scale planetary waves requires more theoretical work; recent progress on this front is discussed by Hendershott (1989) and Hendershott and Miller (1989).

In this communication, we compute free solutions of the shallow-water equations using the finite-element eigencodes developed by Platzman (1978), which have been
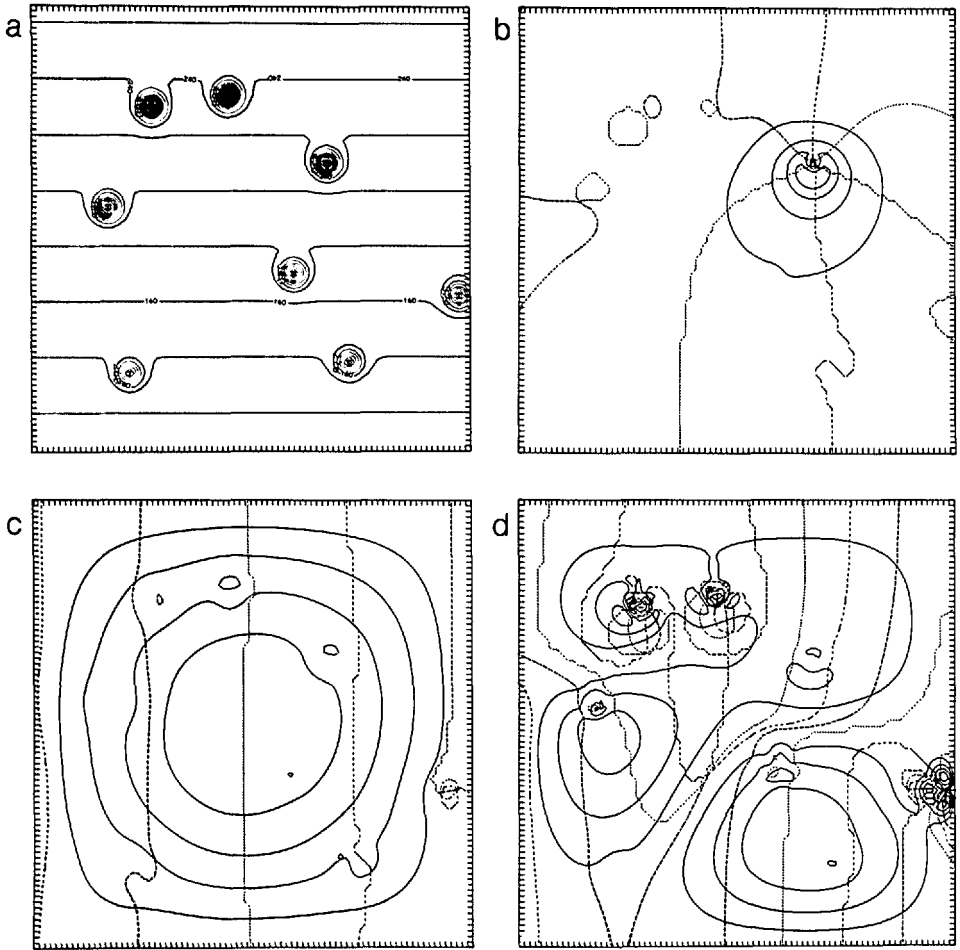
Figure 1. Square basin geometry of Miller (1986a,b) with Gaussian seamounts of 250 km radius and 2500 m height in a 5000 m depth ocean with the planetary vorticity gradient included. A large-scale planetary mode can survive, virtually intact, in the presence of strong topographic variability evident in (a) the f/H contours (Contour interval = $2 \times 10^{-9}\,m^{-1}\,s^{-1}$) for this case. The first 15 normal modes of this system are individual (or coupled) seamount oscillations; the volume-transport streamfunction for the third such eigenmode is shown in (b) (Period = 3.9 days, solid lines are constant amplitude, dashed lines are constant phase). The fundamental planetary mode (period = 8.7 days) appears as the 16th mode of the system (c), but with a longer period than the 8.1-day flat-bottom analogue. Lower-frequency modes in this case are usually either pure seamount oscillations or mixed planetary-topographic modes, e.g., as in (d) the 34th mode with period = 15.6 days. The eigensolutions of other cases of low-frequency, volume-transport flow over well-resolved topography have been discussed by Miller (1986a,b), who provides details of this model.

Journal of Marine Research

Table 1. Geometry and topography for each case.

Geometry	Topography	Resolution
Hemisphere	Flat (3500 m)	Low
Pacific	Flat (3500 m)	Low
Pacific	Flat (3500 m)	High
Pacific	Flat (4400 m) with 2500 m E.P. Ridge	
Pacific	Flat (5000 m) with 2500 m E.P. Ridge	Low
Pacific	SIO Rand	Low
Pacific	SIO Rand	High
Pacific with New Zealand	SIO Rand	High
Pacific with New Zealand and Hawaii	SIO Rand	High
Pacific with New Zealand, Hawaii and Fiji	SIO Rand	High
Reduced Pacific	SIO Rand	High
Reduced Pacific with Hawaii	SIO Rand	High

generously made available for this study (§2). A variety of basin shapes and topographies (Table 1), relevant to the Pacific basin and the 2-day to 6-day period band, are considered in order to aid the interpretation and evaluation of the solutions with realistic geometry and topography. The hemispherical geometry of Longuet-Higgins and Pond (1970) is first addressed (§3), primarily as a test case but also to corroborate and validate the flat-bottom vorticity-mode structures which occur in Pacific-shaped basins (§4). These flat-bottom vorticity modes prove to be useful in interpreting the solutions with topography (§5). In that section, we compare the closed-Pacific solutions with realistic topography with the global solutions of PCHS81 and find substantial similarity between modes with significant amplitude in the Pacific; this result justifies closing off the Pacific basin east of the Drake Passage and between Tasmania and Antarctica.

When Pacific geometry and realistic topography are included in high resolution cases (§5), multiple modes occur bearing similar large-scale planetary-mode structures, which suggest that the large-scale planetary modes are rent by small-scale model vorticity waves as described in (iii). Since it is impossible to properly resolve both the planetary and the topographic waves which would occur in the real ocean (the model topographic waves are smoothed-topography aliases of the real ocean waves), we consider a reduced-area Pacific domain in which unresolved f/H contours of the continental shelf/slopes and the Fiji/New Zealand regions are eliminated; the topography of the interior region is left unfiltered, except at element scale. By this approach, solutions are obtained (§6; Figs.10, 11) which we contend are characteristic of the intrinsic spatial structures and frequencies of the largest-scale planetary-topographic modes of the Pacific. In reality, each normal-mode solution may occur as a family of modes arising from strong interactions with real ocean topographic waves.

Limits on computational power prohibit our predicting the details of such families, if they exist. Even if such families do occur, our predictions can help to interpret observations (§7) of sea-level and bottom pressure (from island/coastal tide-gauges and open-ocean pressure sensors) since we argue in (iii) that the open-ocean, basin-scale structure will be preserved among family members.

2. Platzman's eigenmodel

Platzman (1975; 1978; 1981) has developed a finite-element formulation for computing the normal modes of the linearized, unforced, inviscid, shallow-water equations for arbitrary boundaries on the sphere. The shallow-water equations, viz.,

$$\frac{\partial u}{\partial t} - 2\Omega \sin \theta v = - \frac{\partial \eta}{\partial \phi} \frac{g}{a \cos \theta} \tag{2.1a}$$

$$\frac{\partial v}{\partial t} + 2\Omega \sin \theta u = - \frac{\partial \eta}{\partial \theta} \frac{g}{a} \tag{2.1b}$$

$$\frac{\partial \eta}{\partial t} + \frac{1}{a \cos \theta} \left[\frac{\partial(uH)}{\partial \phi} + \frac{\partial(vH\cos \theta)}{\partial \theta} \right] = 0, \tag{2.1c}$$

where (u, v) are the horizontal velocities, η is the free-surface deflection, H is the fluid depth, g is gravitational acceleration, a is the radius of the earth and Ω is the rotation rate of the earth, under the assumption of no flow through the specified boundaries, are transformed into a discrete matrix eigenvalue problem of the form

$$-iAX = \sigma BX \tag{2.2}$$

where A is a skew-symmetric real operator, B is a symmetric real operator, X is the column eigenvector of (η, φ, ψ), φ is a velocity potential, ψ is a volume-transport streamfunction and σ is the eigenfrequency. A Lanczos method is used to penetrate the spectrum of solutions. The set of FORTRAN programs forms a powerful numerical tool which Platzman has generously made available for this study. The model is applied herein to a variety of geometries and topographies that model the Pacific Ocean (Table 1). We use two levels of resolution, corresponding to mean triangular finite-element areas equivalent to a 4.5° equatorial square (the resolution used by PCHS81) and a 3.1° equatorial square; they are, respectively, referred to in subsequent sections as low- and high-resolution cases.

3. Flat-bottomed hemispherical basin

As a test case, we compute shallow-water modes for the hemispherical geometry of Longuet-Higgins and Pond (1970), hereinafter LHP70. The Lamb parameter, $\epsilon \equiv 4\Omega^2 a^2/gH_o$ is chosen to be 25., such that the ocean has constant depth $H_o = 3500$ m, and the resolution is selected to be equivalent to PCHS81.
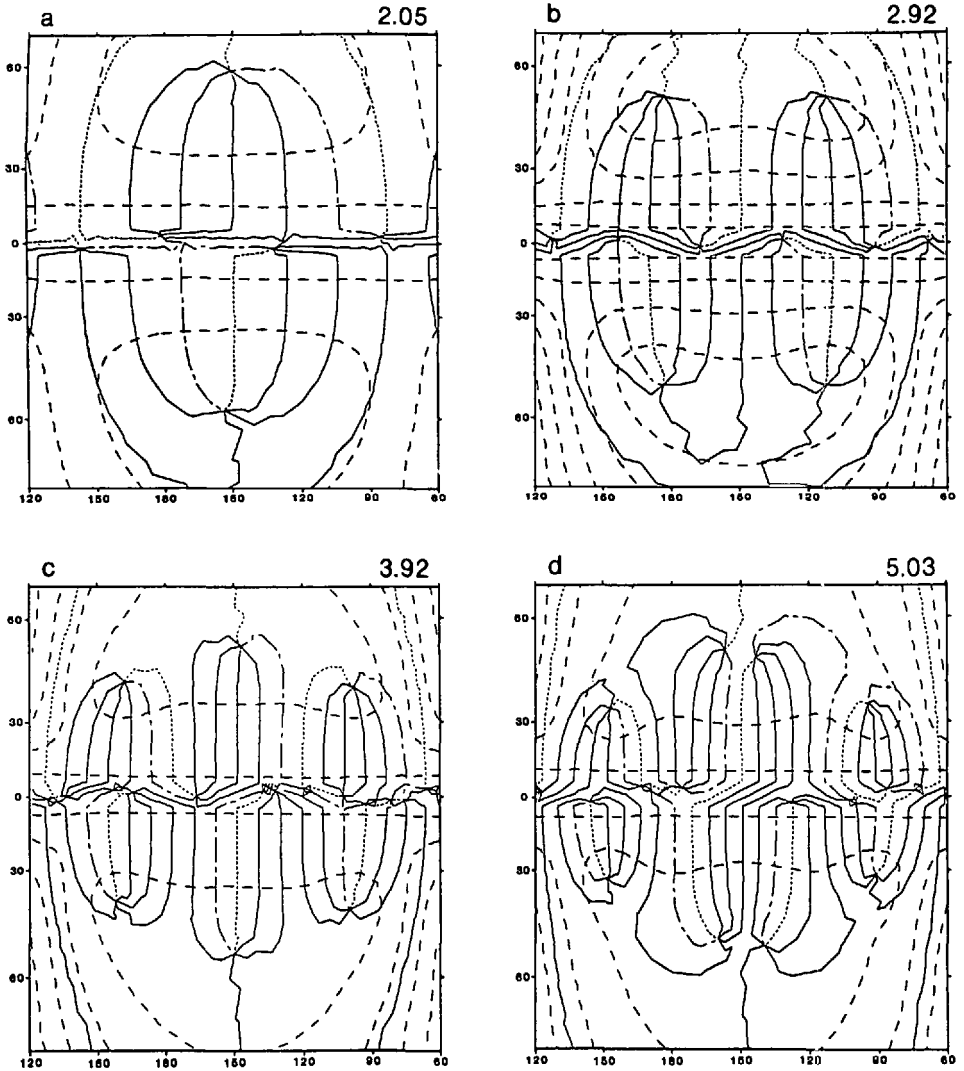
Figure 2. Hemispherical geometry of Longuet-Higgins and Pond (1970) with constant ocean depth of 3500 m and low resolution. Surface elevation, η, of the shallow-water vorticity modes of the system with contours of constant amplitude plotted with long dashes and constant phase with solid lines, except for the "marker" phases which denote the dashed-dot line leads the dotted line. The charts only show structure between 70N and 75S. Eigenperiod, in days, is indicated on the upper right of each plot. (a) Fundamental vorticity mode of the domain, the first antisymmetric mode with period = 2.05 days. (b) Second antisymmetric vorticity mode with period = 2.92 days. (b) Third antisymmetric vorticity mode with period = 3.92 days. (b) Fourth antisymmetric vorticity mode with period = 5.03 days. The quasi-analytical periods found by Longuet-Higgins and Pond are shown in Table 2, for comparison.
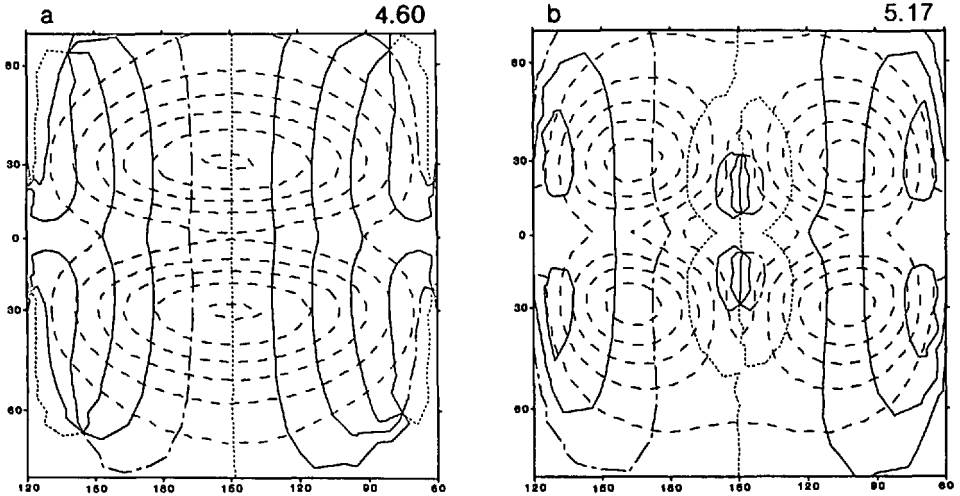
Figure 3. Hemispherical geometry of Longuet-Higgins and Pond (1970) with constant ocean depth of 3500 m and low resolution. Plotted as in Figure 2, but for (a) first symmetric vorticity mode with period ⇨ 4.60 days and (b) second symmetric vorticity mode with period = 5.17 days.

The numerical solutions fall into the distinct and well-known classes of gravity and planetary oscillations, distinguished by the distribution of potential and kinetic (rotational and irrotational) energy in a given mode. Planetary modes are dominated by the rotational component of kinetic energy, being, in this case, always greater than 80% of the total energy. The irrotational component of kinetic energy is less than 1% for all planetary modes except for the fundamental which has 3.8% (Fig. 2a). The gravity modes usually contain less than 10% rotational kinetic energy, although exceptions occur. For example, the fundamental Kelvin mode (not shown), with period 2.02 days, contains 18% rotational kinetic energy, and the three energetic components of the fundamental antisymmetric gravity mode (not shown) are nearly equipartitioned. Typically, however, the gravity modes have more than 40% of their total energy in the irrotational kinetic component and roughly an equal amount in the potential energy component.

The frequencies predicted by LHP70 can be read from their Figure 2, for the modes which bear equatorial symmetry in η, and their Figure 3, for those which are antisymmetric in η. Table 2 shows the periods herein computed vis-a-vis those of LHP70 for the eigenmodes with largest spatial scale; they are grouped according to class, ordered according to period and distinguished according to equatorial symmetry.

The spatial structure of the highest-frequency antisymmetric and symmetric vorticity modes are shown in Figures 2 and 3, respectively. The equatorial symmetries borne out in these plots, combined with the small differences in frequency between

Table 2. Periods of hemispherical basin mode solutions.

Class	Symmetry/mode number	Numerical period (days)	LHP70 period (days)
planetary	A1	2.05	2.0
planetary	A2	2.92	2.8
planetary	A3	3.92	3.8
planetary	S1	4.60	4.5
planetary	A4	5.03	4.7
planetary	S2	5.17	5.0
planetary	S3	5.94	5.7
gravity	S1	2.02	2.0
gravity	A1	1.34	1.3
gravity	S2	1.06	1.0
gravity	A2	0.92	0.92
gravity	S3	0.74	0.73

these computations and the quasi-analytical results of LHP70, suggest that even the low resolution is adequate to model realistic Pacific shape.

4. Flat-bottomed Pacific basins

Next explored is the alteration of eigenmode structure and frequency induced by deforming the hemispherical boundary to that of a Pacific-shaped basin. A constant depth of 3500 m is chosen, as in the hemispherical case, and calculations are performed for both resolutions. The perfectly reflecting horizontal boundaries are specified (slightly differently for the two resolutions) according to the actual shape of the Pacific, except for a wall which closes off the Drake passage and another wall which connects Tasmania and Antarctica. (The effect of excommunicating the Pacific basin from the other ocean basins is discussed at the end of this section.)

Differences in (gravity and planetary) eigenmode structure and frequency between the low- and high-resolution cases are generally small. The highest-frequency vorticity modes appear in a one-to-one correspondence between the high and low resolution cases with one exception. The 7th and 8th highest frequency modes evidently scatter into each other (as discussed, e.g., in section 10 of LHP70), in this case, owing to the perturbation induced by changing the resolution or, perhaps, by the perturbation in lateral boundary structure. Figure 4 shows the high-resolution structure and frequency of the highest-frequency planetary solutions, with the low-resolution period noted in parentheses.

We restrict this discussion to the eight vorticity modes which occur with period shorter than 7 days. The fundamental vorticity mode (Fig. 4a) retains a fairly antisymmetric structure, although most other modes can no longer be simply classified according to equatorial symmetries. Note that the higher frequency vorticity modes can have significant nonzero (Larichev, 1974; Flierl, 1977) and variable amplitude along the coast, since $\sigma/(2\Omega \sin \theta)$ is not vanishingly small.
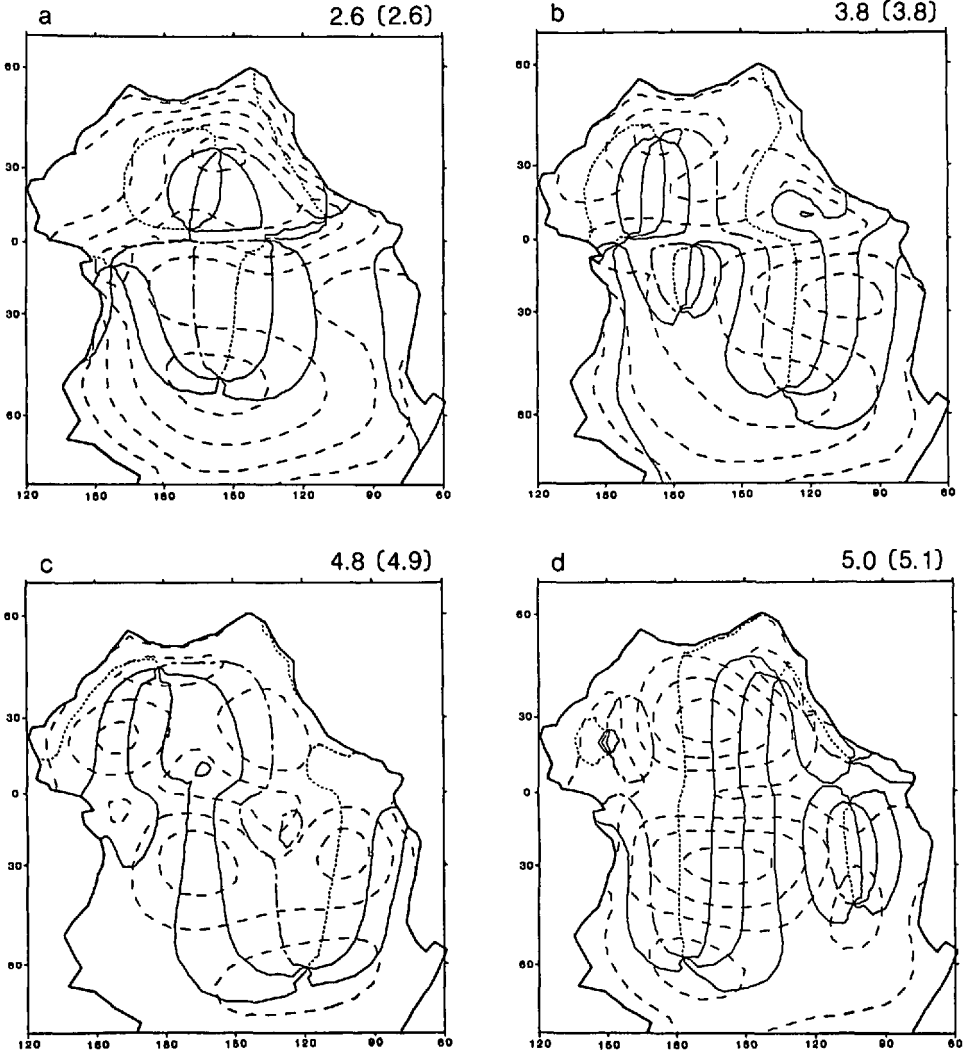
Figure 4. Pacific geometry with constant ocean depth of 3500 m and high resolution. Plotted as in Figure 2. (The edge of the charts at 75S is NOT a boundary of the basin.) (a) Fundamental planetary mode with period = 2.6 days. (b) Second planetary mode with period = 3.8 days. (c) Third planetary mode with period = 4.8 days. (d) Fourth planetary mode with period = 5.0 days. (e) Fifth planetary mode with period = 5.8 days. (f) Sixth planetary mode with period = 6.3 days. (g) Seventh planetary mode with period = 6.8 days. (h) Eighth planetary mode with period = 7.0 days. Periods in parentheses are for the low resolution analogues. The (#) denotes the two high resolution modes which are mixed versions (see the text) of the two low resolution modes with periods 7.2 days and 7.4 days.
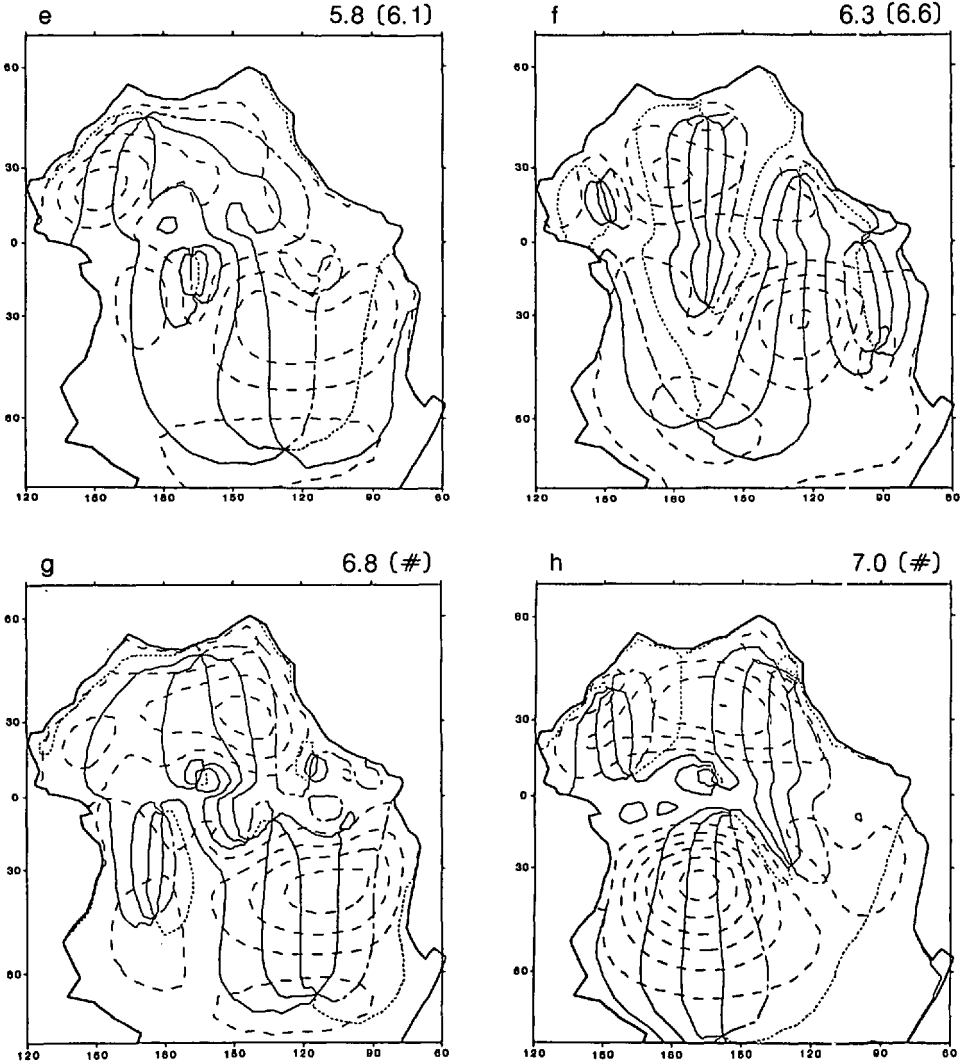
Figure 4. (Continued)

It is interesting to compare these results with Longuet-Higgins' (1971), hereinafter LH71, who estimated the frequencies of Pacific-basin, flat-bottom modes by reducing the LHP70 frequencies, which are proportional to the basin dimensions. Since LH71 chose 3500 m as the representative depth of the Pacific, his estimates are directly comparable with the results of the present solutions. LH71 estimated the period of the fundamental antisymmetric planetary mode to be 2.9 days, compared to 2.6 days found here for the full geometry. His estimate of the fundamental symmetric (fourth-highest frequency in LHP70) planetary mode period was 6.7 days, compared to 5.0 days found here for the first symmetric (fourth highest-frequency; Fig. 4c)

mode. Although LH71 estimates a period (4.2 days) for the second antisymmetric mode, the corresponding mode found here (period 3.8 days) is not purely antisymmetric, rather being a mixture of symmetric and antisymmetric structures.

Platzman (private communication, 1984) has computed flat-bottom global normal modes for periods as long as 4.0 days. This allows a comparison of the present closed Pacific-basin results with global solutions. Using a constant depth of 3948 m, Platzman found only 3 modes which could be classified as vorticity oscillations. The longest-period flat-bottom mode of those computed was displayed by PCHS81 in their Figure 8. This 4.0-day period global vorticity mode has clear correspondence in spatial structure (except in the southwestern Pacific) and in frequency with the 3.8-day mode found here (Fig. 4b). Furthermore, the fundamental flat-bottom global vorticity mode (not shown) has the same period (2.6 days) as found here and has Pacific-basin structure which is extremely similar to Figure 4a. A discrepancy arises, however, in that Platzman's unpublished flat-bottom global solutions contain a vorticity mode (period 3.3 days) which has no counterpart in the present flat-bottom closed-Pacific solutions. That mode has circumglobal energy flux and significant energy density in all the ocean basins. Topography can be expected to seriously interrupt such circumglobal energy transport, which suggests that closed-Pacific results are meaningful. In particular, the Pacific Antarctic Rise and East Pacific Rise may act to cordon off the South Pacific basin, forming sub-basins as suggested by Rhines (1969) and Anderson and Killworth (1977). Indeed, as discussed in §5*b.i*, the global vorticity-mode solutions of PCHS81 compare favorably with the present closed-Pacific solutions when realistic topography is included.

5. Pacific basins with topography

a. Model East Pacific Rise

As a prelude to exploring the case of realistic topography, two cases are examined that include topography which models the Pacific Rise ridge system, the dominant large-scale topographic feature of the Pacific. The model ridge is constructed by specifying a line of latitude-longitude points, representing the "backbone" of the ridge, chosen to roughly follow the observed ridge spine. Then an array of topography is constructed on a 1° grid by computing the height of each array point based on its absolute distance from the closest spinal point of the ridge. A Gaussian ridge profile, which decays perpendicularly to the ridge spine with a decay scale of 500 km, is chosen as fairly representative of the observed ridge. Two cases were examined (Table 1), one with a ridge height of 2500 m in an ocean with otherwise constant depth of 4400 m and the second case with constant depth set to 5000 m and the same ridge. The resulting pattern of (f/H) for the latter case is shown in Figure 5a. The ridge supports topographic waves which have similar structure but different frequencies for these two cases, such that a resulting planetary-topographic mode of one of the two cases is likely
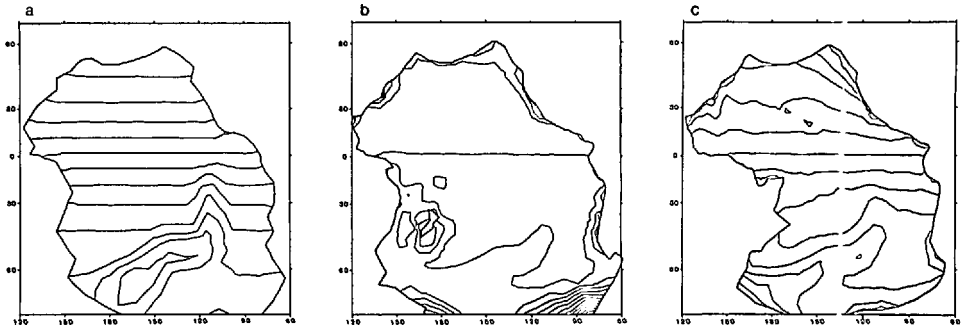
Figure 5. Contours of constant f/H in model Pacific basins for (a) 2500 m-high model Pacific Rise in an otherwise constant depth ocean of 5000 m depth (CI $=$ 5.2 $\times$ 10^{-9} m^{-1} s^{-1}), (b) Rand/SIO topography smoothed to the high resolution of the eigenmodel (CI $\approx$ 2.9 $\times$ 10^{-8} m^{-1} s^{-1}), and (c) Rand/SIO topography smoothed as in (b) but reduced-Pacific geometry such that the near-coastal and Fiji/New Zealand regions of steep and poorly resolved f/H are excised from the domain (CI = 7.3 $\times$ 10^{-9} m^{-1} s^{-1}).

to be structurally similar to an analogue mode in cases with realistic topography. Such comparisons help to interpret the large-scale responses discussed later in this section and in §6.

An important point is exposed in these model ridge calculations. The planetary-mode activity in the North Pacific basin may interact strongly with ridge-mode activity, associated with the East-Pacific Rise, in the South Pacific basin (Fig. 6). The equator forms no barrier to such coupling, so that rending (Miller, 1986a) of North Pacific, shallow-water planetary-like modes by South Pacific topographic-wave inter-action may occur.

b. Rand/SIO topography

i. Low resolution. In order to include realistic topographic variability in these calculations, the 1° resolution Rand/SIO topography was obtained from S. M. Smith of Scripps. A direct comparison can be made between the present closed-basin results and the global solutions of PCHS81 because the topography and resolution are identical. Differences in geometry between this low-resolution case and that of PCHS81 include the somewhat different choices of boundary points which define the Pacific (as in the flat bottom cases, the Drake Passage is closed and Tasmania is connected to Antarctica) and the present exclusion of New Zealand as an island (it is here treated as a shallow sea of 50m depth). The exclusion of New Zealand results in several spurious topographic modes (over New Zealand) which are easily identified by their absence from the spectrum of PCHS81; these are henceforth excluded from the discussion. Modes which occur in the spectrum of PCHS81 faithfully appear here, except they often have structural differences localized around the New Zealand
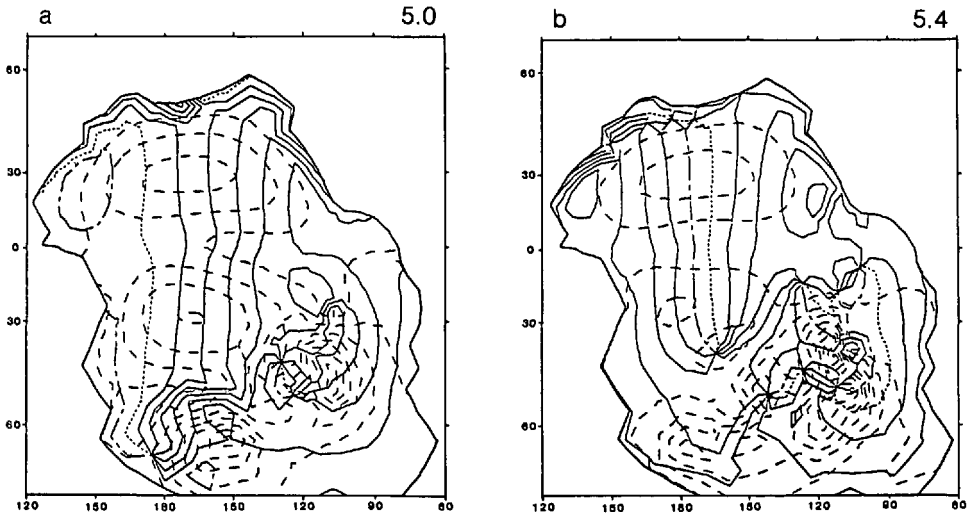
Figure 6. Pacific geometry with 2500 m high model Pacific Rise in an otherwise 4400 m deep
ocean. Example of the rending of the planetary mode of Figure 4d by interaction with ridge
modes of the South Pacific. Plotted as in Figure 2 for (a) mode with period = 5.0 days and (b)
mode with period = 5.4 days.

region. (Cf. the similar situation when resolving New Zealand in the high resolution
cases of §5*b.ii.*)

The present Pacific-basin results are next compared and contrasted with the global
solutions obtained by PCHS81 and the supplementary modes shown by Platzman
(1985), hereinafter P85. The fastest vorticity mode occurs as a topographic wave
around the New Zealand Plateau with period 2.01 days and entirely analogous to the
topographic wave which appears in two modes (periods 1.58 and 1.61 days) computed
by PCHS81. In the present solution as well as PCHS81, this vorticity wave weakly
excites (cf. Brink, 1986) basin-scale structure comparable to the fundamental gravity
(Kelvin-like) mode of the Pacific which appears with principle resonance as a separate
mode with period 1.68 days in the present results and with period 1.49 days in
PCHS81.

The second (2.50 day period) and third (2.82 day period) vorticity modes of this case
are very similar to the modes with period 2.44 days and 2.75 days of PCHS81 (see also
Fig. 7a, b). Although the details of modal structure over the New Zealand region differ
with PCHS81, both modes bear general structure in the North Pacific and period
suggestive of the 2.6-day flat-bottom fundamental planetary mode (Fig. 4a), although
PCHS81 noted their 2.44-day mode was trapped to the Hawaiian ridge, based on the
energy-flux diagnostic. As discussed later, the 2.50-day mode is indeed extinguished
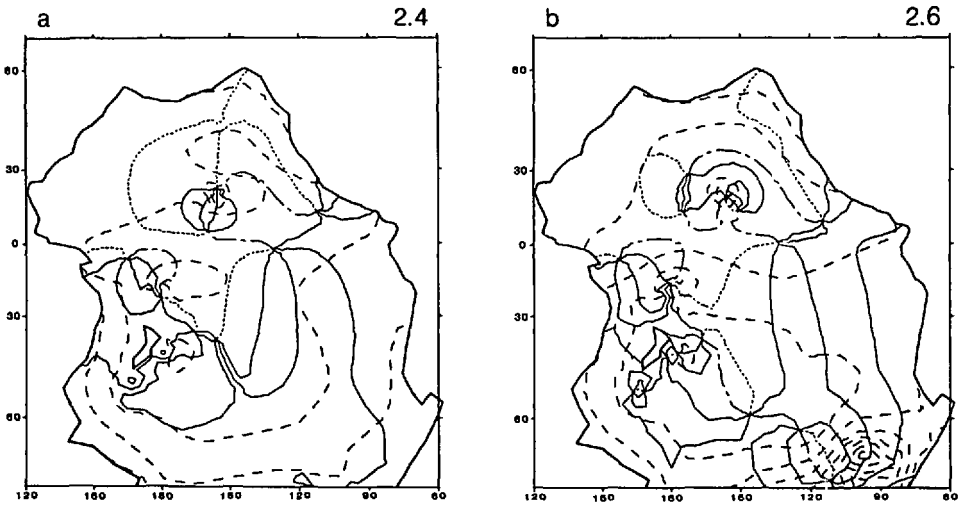when Hawaii is resolved in the high resolution cases.

Figure 7. Pacific geometry with Rand/SIO topography and high resolution. Plotted as in Figure 2, but for (a) large-scale vorticity mode with period ≈ 2.4 days and (b) large-scale vorticity mode with period = 2.6 days. The mode in (a) is extinguished when Hawaii is resolved with one grid element. The mode in (b) remains intact, even if the Fiji Islands are resolved as well, and takes on period (2.7 days) and structure similar to Figure 4a and Figure 10 by losing the amphidromic pair seen over Hawaii in (b).

The fourth mode encountered (3.57 days period) has an obvious counterpart (3.59 day period) in P85's results. Although the structure (Fig. 8a) matches almost exactly that of the P85 mode, Platzman's mode remarkably appears to be overwhelmingly controlled by a topographic-wave resonance of the Kerguelan Plateau in the South Atlantic. Inspection of the two cases with model ridges reveals that each case has a planetary-ridge mode which resembles the 3.57-day mode in South Pacific structure and in frequency. The fourth mode thus appears to be a planetary-topographic wave of the South Pacific basin. The fundamental ridge mode (see Fig. 9a), supported by the northern slope of the Pacific Antarctic Rise, occurs as the fifth mode of this closed-Pacific case, with period 3.95 days. In P85 the fundamental ridge-mode structure appears in three modes, with periods of 3.83, 4.00, 4.13 days, owing to coupling with remote topographic waves of other ocean basins.

The sixth vorticity mode (4.34 day period) is suggestive of the 4.43-day period mode which appears in P85 (see also Fig. 11a). The planetary-like structure in the North Pacific of the two modes is similar, but the South Pacific structure in Platzman's mode is more strongly influenced by the second ridge mode (see Fig. 9b) of the Pacific Rise. The few remaining modes of the 4-6 day period band in both cases are dominated by the second ridge mode and Fiji/New Zealand topographic waves. Since the resolution is insufficient to reasonably resolve those regions we cannot further compare these two cases with any confidence. But the correspondence between our vorticity modes and
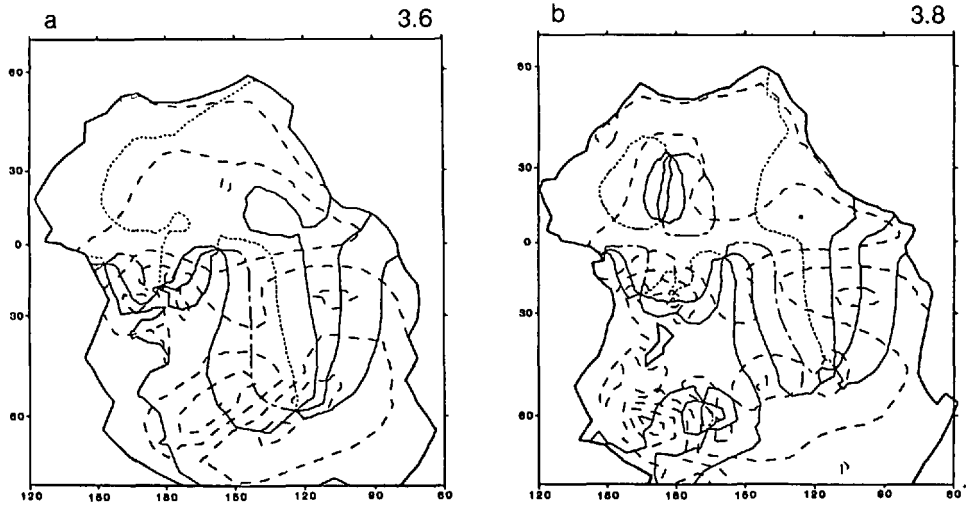
Figure 8. Pacific geometry with Rand/SIO topography. Plotted as in Figure 2, but for planetary-topographic mode of the South Pacific for (a) low resolution case with period = 3.6 days and (b) high resolution case with period = 3.8 days.

those of P85 suggests that the results in closed Pacific basins with realistic topography are meaningful.

ii. High resolution. Four cases with high resolution are examined, differing only in the "islands" resolved in the interior ocean. The first case has no interior islands; even New Zealand is treated as a shallow sea. The second case resolves New Zealand with 6 grid elements, the third case additionally resolves Hawaii with one element and the final case additionally resolves the Fiji Islands with one element. By incrementally resolving "islands," it is possible to determine which modes are controlled by poorly resolved topographic features. For example, in the case with no islands, there again occur (cf. §5b.i) several spurious topographic modes around New Zealand which are extinguished when the New Zealand Island is resolved.

These cases better resolve the *f/H* contours and consequently admit topographic vorticity waves with smaller scale and higher frequency. Several topographic waves with periods less than 2.1 days in the vicinity of the New Zealand region tend to weakly excite the large-scale gravity modes at off-resonance (cf. Brink, 1986). Subsequently, modes which are clearly small-scale (and probably poorly resolved) topographic waves are ignored unless they strongly affect structure of the large-scale modes.

In the case which resolves only New Zealand, the two highest-frequency large-scale vorticity modes (Fig. 7) occur with structure and frequency (2.45 and 2.60 days) very similar to the two analogous low-resolution modes. The 2.60-day mode in this case is coupled to a topographic wave on Antarctica, near the Bellinghausen Sea, which occurs as a nearly pure topographic wave with period 2.62 days as well. The impact of
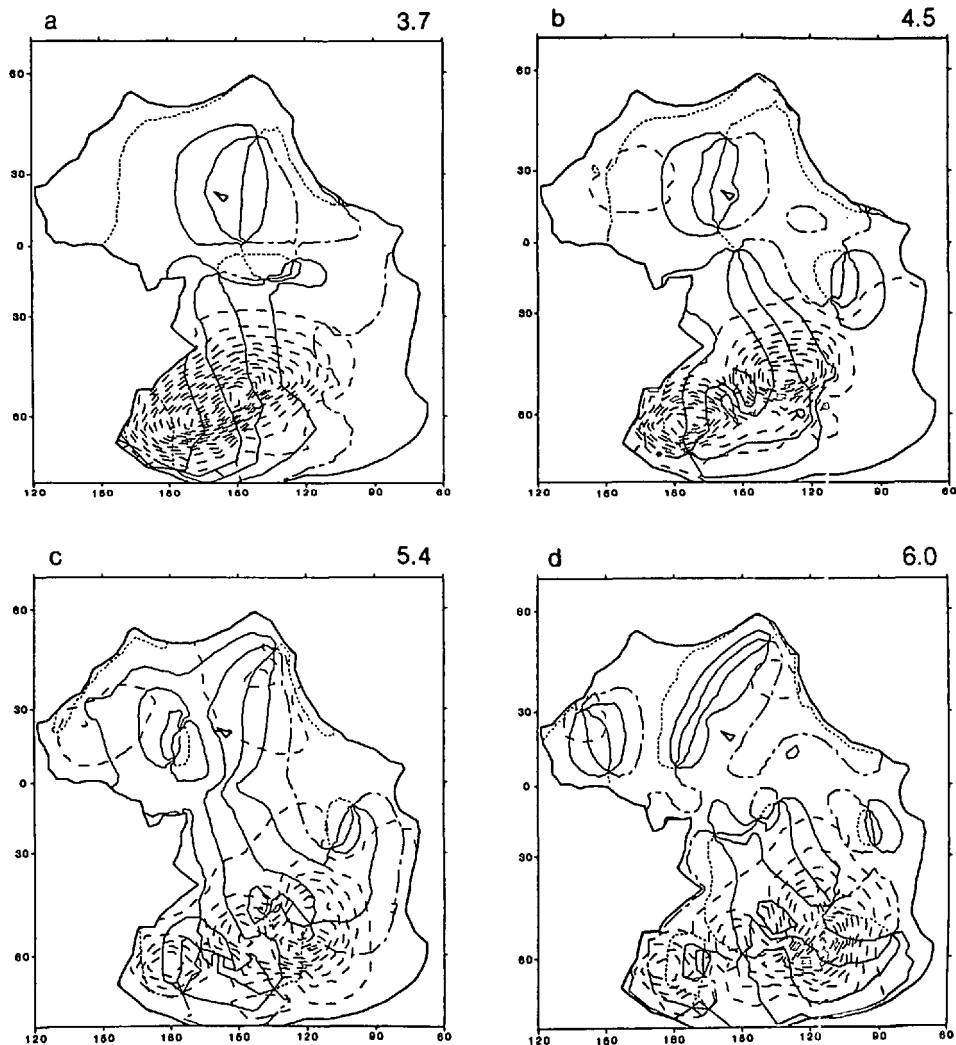
Figure 9. Reduced-Pacific geometry with Rand/SIO topography and high resolution. Plotted as in Figure 2, but for the ridge modes of the Pacific Rise. (a) Fundamental ridge mode with period = 3.7 days. (b) Second ridge mode with period = 4.5 days. (c) Third ridge mode with period = 5.4 days. (d) Fourth ridge mode with period = 6.0 days.

resolving New Zealand is minute for both modes, resulting in only local changes in structure and virtually no change in frequency. When the Hawaiian Island chain is resolved with one grid element, however, the 2.45-day mode is extinguished. The 2.60-day mode shifts to a 2.55-day period and loses the amphidromic pair that is located very close to Hawaii in Figure 7a, but retains its large-scale structure which is reminiscent of the fundamental flat-bottom vorticity mode of Figure 4a. PCHS81 suggested that the Fiji Plateau controlled their analogue of the 2.60-day mode, but

resolving the Fiji Island region does not destroy this mode. What is extinguished is a mode with period 2.95 days (not shown) that was trapped to Fiji and exhibited weak basin-scale structure akin to the fundamental flat-bottom planetary mode. Thus, when New Zealand, Hawaii and Fiji are all resolved, the 2.60-day mode shifts to a 2.72-day period and exhibits basin-scale structure very similar to the fundamental flat-bottom vorticity mode of Figure 4a.

The fundamental ridge mode of the Pacific Antarctic Rise (see Fig. 9a) in these cases occurs with higher frequency (3.6 day period) than for the low resolution cases. The second ridge mode (see Fig. 9b) also occurs with higher frequency (4.0 day period) compared to P85 (4.58 day period) and the low resolution closed Pacific case (4.97 day period). The consequence of these shifts to high frequency is to cause the analogue of the 3.57-day low-resolution South Pacific planetary-ridge mode (Fig. 8) to exhibit structure along the ridge which is more like the second ridge mode than the fundamental ridge mode. The impact on this mode of resolving the different "islands" is mainly in the phase organization in the North Pacific where the amplitude is rather weak.

Longer-period modes which bear large-scale planetary-mode structure in the North Pacific exhibit multiple occurrences which suggest that families of modes are formed, as discussed by Miller (1986a). The perturbations induced by resolving New Zealand and the other islands can often distort the topographic waves and shift frequencies which result in a change in the particular interaction among topographic waves and planetary response. Thus, further discussing the solutions obtained for the high resolution case is an arduous task. However, the large-scale planetary-mode and ridge-mode structures which do occur in the North Pacific and South Pacific, respectively, are robust. Therefore, the next task is to expose those large-scale planetary-topographic mode structures which are intrinsic to the Pacific.

6. Reduced-Pacific basin

As seen in §5, the interaction between large-scale planetary waves and smaller-scale topographic waves can result in families of modes bearing characteristics of both types of waves. But oceanic topographic waves are inevitably poorly resolved when simultaneously attempting to resolve the planetary-scale waves; model topographic waves are smoothed-topography aliases of the real topographic waves. To suppress those poorly resolved topographic waves, consider a Pacific basin of reduced size wherein the boundaries exclude the near-coastal topographic variations bearing length scales at the limit of resolution. We contend that the modes of this model framework will characterize the structure and frequencies of modes which arise from the large-scale f/H gradients. These characteristic modes may still occur as families in the real ocean, but the members will tend to exhibit similar open-ocean structure away from the topographic features that support the interactive waves (Miller, 1986a).

The Pacific topographic regions most difficult to resolve appear to be the Fiji

Plateau, the New Zealand Plateau and the numerous surrounding deep trenches and island chains. Isolated seamounts and short island chains in the open ocean are unlikely to interact strongly with large-scale planetary-wave activity (see Fig. 1); these have already been removed by the element-scale filtering of PCHS81. Thus boundaries for a reduced-Pacific domain (compare Fig. 5c with 5b) are chosen to exclude steep (f/H) regions near boundaries, to excise the entire Fiji Basin and Tasman Sea from the domain and to resolve the Hawaiian Island chain with one grid element. If planetary waves can propagate intact through the Fiji region the modes discussed are likely to have somewhat shorter periods than found here (Longuet-Higgins, 1964) and bottom roughness may add to that effect (Rhines and Bretherton, 1973; comment i of §1).

For the reduced-Pacific domain, the dominant topographic modes are the Pacific Antarctic Rise ridge modes (Fig. 9), which can interact strongly with the planetary mode structures. Although the frequencies of these ridge modes are somewhat comparable to the analytical solutions of ridge modes discussed by Rhines (1969), Anderson and Killworth (1977) and Ripa (1978), it is difficult to compare them in detail. This is because the Rise geometry is neither straight nor longitudinally oriented and because the Coriolis parameter, f, is fully variable (neither f-plane nor β-plane). The latter effect modulates the strength of the topographic effects and can set intrinsic along-ridge length scales which are not necessarily those imposed by the geometry of the problem (see, e.g., Figure 7 of Miller, 1986a). Rhines and Bretherton (1973) show that an upper-bound on the frequency of planetary-topographic waves in a basin is

$$\sigma \leq \left| H\left(\widehat{\frac{f}{H}}\right)\right|_{max},$$

where the carat indicates deviation from the mean. Along, say, 55S with constant $f = 1.2 \times 10^{-4} \text{s}^{-1}$, the East Pacific Rise shoals roughly at 3000 m depth from a 4500 m average, which implies a lower-bound period[2] for the fundamental ridge wave of $O(1.8 \text{ days})$, compared to the $O(3.7 \text{ day})$ period found here. The β-effect can act to perturb the (f-plane) ridge mode periods to higher or lower values depending on the direction of the modal phase propagation. The fundamental ridge mode (Fig. 9a) propagates phase west-southwestward and therefore occurs with higher frequency than would its f-plane analogue; the structure is coincidentally quite similar to that of a shelf mode shown by Miller (1986a; his Fig. 4a). The second ridge mode (Fig. 9b) propagates phase similarly but with two amplitude maxima along the northern flank of the Rise. The third and fourth ridge modes (Fig. 9c,d) have three amplitude maxima along the northern flank but exhibit a significant "mode-1" amplitude maximum on the southern flank, where northeastward phase propagation occurs. In (unpublished) quasigeostrophic and/or volume-transport flow computations with well-resolved
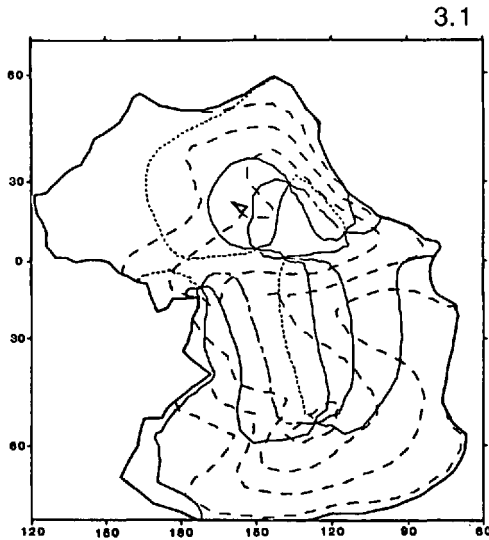
3.1

Figure 10. Reduced-Pacific geometry with Rand/SIO topography and high resolution. Plotted as in Figure 2, but for the fundamental planetary-topographic mode of the Pacific with period ⇌ 3.1 days.

ridges, similar types of scenarios can occur wherein the response on one side of a ridge can be coupled to differing structures on the other side. For the problem at hand, the ridge modes shown in Figure 9 form a set of topographic modes which may interact with the planetary-mode structures in the 3-6 day period band, discussed next.

For the reduced-Pacific domain of Figure 5c, there occur five basin-scale modes in the 3–6 day period band which have significant amplitude in the North Pacific. The fundamental vorticity mode for this case is shown in Figure 10. It is analogous to the fundamental planetary mode of the flat-bottom case (Fig. 4a), although the period is shifted from 2.6 days to 3.1 days apparently due to the shrunken domain. For the full-Pacific topographic case which resolves New Zealand, Hawaii and Fiji, there is a mode (not shown) similar to Figure 10, but with period 2.7 days; the amphidromic point which occurs halfway between Hawaii and San Francisco in Figure 10 occurs about 10° north of Hawaii in the full-Pacific domain. As inferred from the results of the sequence of island-resolving full-Pacific cases, the fundamental vorticity mode of the full-domain cases can be rent into a family of modes (e.g., Fig. 7), due to coupling with poorly resolved Hawaiian-Island and/or Fiji-Island topographic waves. (If Hawaii is left unresolved in the reduced-Pacific case, a localized topographic wave occurs which is of sufficiently short period (2.5 days) to fail to couple to the 3.1-day basin-scale oscillation.) This 3.1-day mode may correspond to Luther's (1980) observation of a basin-scale coherent 3-day signal among certain Pacific Ocean sea-level observations, although the predicted 3-day period may be fortuitous because of the frequency shift induced by the shrunken model domain.
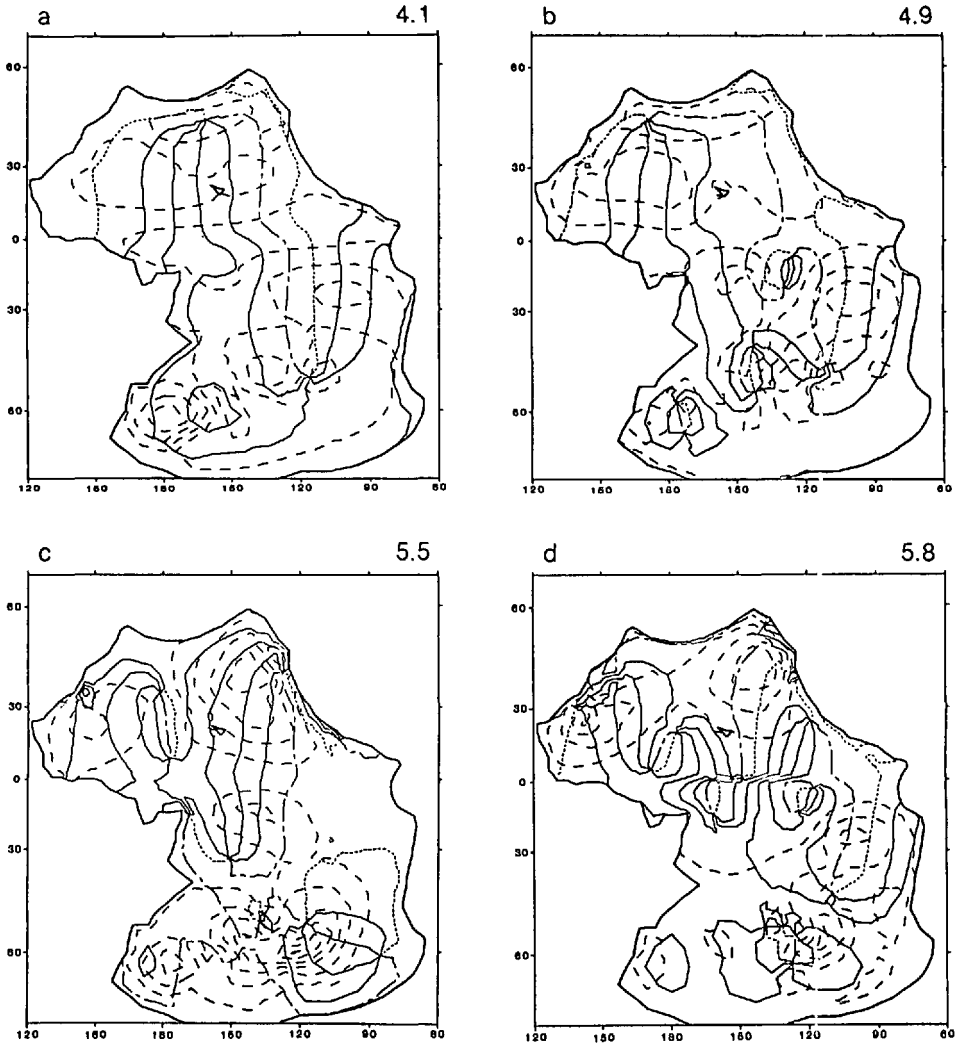
Figure 11. Reduced-Pacific geometry with Rand/SIO topography and high resolution. Plotted as in Figure 2, but for the (a) second planetary-topographic mode with period ⸱ᵓ 4.1 days, (b) third planetary-topographic mode with period = 4.9 days, (c) fourth planetary-topographic mode with period = 5.5 days, (d) fifth planetary-topographic mode with period = 5.8 days.

The second basin-scale vorticity mode in the reduced-Pacific geometry (Fig. 11a) has a period of 4.1 days and some similarity with the 3.8 day flat-bottom planetary mode, except for the excitation of the second ridge mode (Fig. 9b) of the Pacific Antarctic Rise in the South Pacific. The North Pacific planetary-wave structure of this mode is the dominant contributor to the planetary structure seen in the 4.4-day period mode of P85, the 4.3-day mode of the low resolution Pacific geometry, and several modes, with roughly 4.3 day periods, associated with the high-resolution geometry. In

the case with an otherwise 5000 m depth ocean and with the model East Pacific ridge, a mode occurs with similar basin-scale structure and 3.7-day period.

The third basin-scale vorticity mode of this geometry (Fig. 11b) has a period of 4.95 days and somewhat resembles the flat-bottom planetary mode with period 4.8 days, although coupling to the third ridge mode (Fig. 9c) occurs. The fourth and fifth basin-scale modes in this case (Fig. 11c, d) are influenced by the large-scale sloping bathymetry of the Northeast Pacific. The North Pacific structure of these two modes appears repeatedly, with similar periods, in families of modes which occur in the full Pacific domain. The 5.5-day mode has cross-equatorial structure which does not change phase, which suggests that this mode is a descendent of the 5.0-day nearly-symmetric flat-bottom mode (Fig. 4d). The structure in the South Pacific, however, is influenced by the third and fourth ridge modes of the Pacific Rise. The 5.8-day mode has no unambiguous counterpart in the flat-bottom geometry.

These results suggest that the structure exhibited by the four prototype basin-scale modes in the 4–6 day band contribute to the basin-scale coherent sea-level signals observed by Luther (1980; 1982). Based on the high resolution results, wherein it is possible to monitor the stability of modes to the island perturbations as well as the number of occurrences of family members, the 4.1-day mode and the 5.5-day mode will most likely be the dominant contributors. The results also suggest that a bottom pressure record from the South Pacific, along the East Pacific Rise, will be coherent with (nonamphidromic) tide gauges in the North Pacific for the eigenfrequencies of the real ocean.

7. Observational prospects

The large spatial scales and small amplitudes of basin-scale planetary waves suggest that detection will probably be solely associated with tide gauges and bottom-pressure sensors. For example, the velocity field associated with quasigeostrophic wavelengths of $O(10000$ km) and $O(1$ cm) amplitude in the midlatitudes is only $O(0.5$ mm/s). Deep-ocean current meter records from the NEPAC (Hu and Niiler, 1987) deployments (42N and 28N, 152W) in the Northeast Pacific indicate that local ambient velocity signals in the 2–6 day band are approximately one order of magnitude larger than those expected from basin mode excitation. Note, however, that ocean acoustic tomography, which may be able to measure the time variability of *spatial averages* of barotropic currents, provides a technique for filtering the small-scale components of velocity in the relevant frequency band. Lawrence and Spiesberger (1989) have tested the feasibility of this measurement technique be detecting, with tomographic methods, the velocity fields associated with resonant basin modes which can be excited by the mesoscale turbulence of Gulf Stream regions in numerical models (Miller *et al.,* 1987). Spiesberger (private communication, 1988) is analyzing tomographic records from the eastern Pacific for the characteristics of the ambient spatially averaged, fluctuating, barotropic velocity field.

Significant temporal coherence in the 4–6 day period band has been detected over basin scales among coastal and island tide-gauge stations in the Pacific (Groves and Zetler, 1964; Groves and Hannan, 1968; Luther, 1980, 1982). Luther (1980) also observed, between a few Pacific stations, significant coherence over basin scales for periods near 3 days. A thorough study of the numerous tide-gauge records available requires contemporaneous records of atmospheric pressure at each station so that subsurface pressure, the dynamic component of the oceanic signal, can be estimated. The present computations suggest that the 3-day wave (Fig. 10) is the fundamental planetary mode of the Pacific and that several distinct modes (Fig. 11) should be resolvable in the 4–6 day period band. The results also suggest that observations of the spatial distributions of sea-level variance and coherence phase should include both open-ocean as well as coastal stations in the analysis of the subdivided frequency bands.

Further corroborative data are being analyzed as part of BEMPEX (Luther *et al.*, 1987), an experiment which took place in the north-central Pacific. The open-ocean bottom-pressure records which were obtained over a year-long interval will provide a good indicator of large-scale barotropic pressure fluctuations and may suggest the presence of basin-mode signals. Their measurements also provide a large-scale open-ocean benchmark for comparing with modeled barotropic oceanic response to observed atmospheric forcing.

A final source of possible detection is remarkably in the CODE-1 and CODE-2 records of bottom pressure and the contemporaneous sea-level records along the northern California coastline where Davis and Bogden (1989) have statistically isolated the coastal (local) oceanic response to both local and remote forcing. The remotely driven response of sea level and bottom pressure was found to be dominated by a barotropic, nonisostatic signal in the 2–10 day period band. That signal was indistinguishable from an $O(1\ \text{cm})$, uniform, rise and fall of sea level over the entire CODE alongshelf and cross-shelf array, as well as over an $O(900\ \text{km})$ alongshore array of coastal tide gauges. They discussed the large-scale response in terms of "Kelvinlike" barotropic waves and suggested that its presence had probably contaminated previous estimates, obtained from sea-level variability, of coastal-trapped waves, which were also identified in their analysis. The disparity in frequency, however, between the fundamental Pacific Kelvin-like mode (PCHS81 computed a 36 hour period) and the large-scale response suggests that the scattering mechanism[3] described by Brink (1986), whereby coastally trapped, topographic vorticity waves weakly scatter energy

3. Brink's scattering formulation, moreover, is based on a small correction to the $O(1)$ coastal-trapped wave, while Davis and Bogden observed both an $O(1)$ "Kelvinlike" and $O(1)$ coastal-trapped wave response. Also, the theoretical scattered wave is forced by and hence should be coherent with the coastal-trapped wave, but the observed "Kelvinlike" response is incoherent with the coastal-trapped response. Actually, Brink's (1986) scattering mechanism is evident in the solutions of PCHS81 as well as those (not otherwise discussed) here, but the weak excitation of Kelvinlike, or other, gravity modes occurs only for topographic vorticity waves with periods of 50 hours and shorter.

into barotropic Kelvin waves, is an unlikely explanation for this large-scale response. Alternatively, consider that the present computations predict nonzero sea-level displacement and nearly uniform phase along the California coast for the 3.1, 4.1 and 4.9 day basin modes and that Luther's (1982) amplitude estimate of the 4–6 day, Pacific, planetary mode was $O(0.5$ cm$)$. The Davis and Bogden (1989) observations may therefore represent the California coastal signature of Pacific basin vorticity modes, first detected by Groves and Zetler (1964) in the cross-spectrum of sea-level records from San Francisco and Hawaii.

8. Summary

Free linear solutions of the barotropic shallow-water equations are obtained for basin shapes and topographies relevant to the Pacific Ocean. Vorticity modes occur for periods longer than about 35 hours. We seek vorticity modes which are significantly controlled by the (basin-scale) planetary-vorticity gradient in spite of the presence of strong (smaller-scale) topographic gradients.

Results from idealized basins provide useful guidelines for interpreting results from realistic geometry. In Pacific basins with realistic topography, large-scale planetary-like flows are evident but often are obscured because of interactions with smoothed-topography aliases of oceanic topographic vorticity waves. In order to expose the characteristic structures of the large-scale planetary-topographic waves, we consider a Pacific basin with realistic topography, but which has been reduced in size to excise poorly resolved regions of steep (f/H). We find five vorticity modes (Fig. 10, 11) with basin-scale structure within the 3-day to 6-day period band, wherein large-scale coherency has been observed among tide-gauge records. Since similar structures occur in the full-Pacific geometry (with or without topography), we argue that these modal structures are intrinsic features of the large-scale planetary-topographic modes of the Pacific.

A predicted basin-scale mode may interact strongly with smaller-scale topographic waves to form a family of modes within which the members have both similar frequency and similar open-ocean structure away from the relevant topographic feature. Such behavior was also found by Miller (1986a) in high-resolution quasigeostrophic computations with well-resolved topography. Without a better understanding of the impact of smooth-topography aliases of oceanic topographic waves, we cannot predict the number of members in such families or the distortions of the open-ocean structure arising from the topographic interaction. We do find, however, that the dominant large-scale topographic feature, the East Pacific Rise/Pacific Antarctic Rise ridge system, of the South Pacific supports topographic waves which interact with planetary-wave response in the North Pacific.

We argue that these planetary modes are physically meaningful because they may (i) help to clarify the interpretation of observations from island/coastal tide-gauges, open-ocean pressure sensors, and tomographic transponders, (ii) be resonantly excited

by, and hence provide an energy sink for, radiating unstable current regions (Miller *et al.*, 1987) and leaky topographic waves and (iii) lead to a direct estimate of the strength of the friction which acts upon barotropic Rossby waves, if a resonant peak can be unambiguously identified in a power spectrum of sea level. Although our results suggest that the barotropic response to atmospheric forcing in the Pacific Ocean can contain large-scale planetary oscillations, their energetic importance in the 2-day to 10-day period band must be assessed by further studying the relevance of smoothed-topography aliases of oceanic topographic waves and by comparing observations of open-ocean barotropic flows with model flows forced by observed atmospheric variables.

REFERENCES

Anderson, D. L. T. and P. D. Killworth. 1977. Spin-up of a stratified ocean, with topography. Deep-Sea Res., *24,* 709–732.
Brink, K. H. 1986. Scattering of long coastal-trapped waves due to bottom irregularities. Dyn. Atmos. Oceans, *10,* 149–164.
Christensen, N., Jr. 1973. On free modes of oscillation of a hemispherical basin centered on the equator. J. Mar. Res., *31,* 168–174.
Davis, R. E. and P. S. Bogden. 1989. Variability on the California shelf forced by local and remote winds during the Coastal Ocean Dynamics Experiment. J. Geophys. Res., *94,* 4763–4783.
Flierl, G. R. 1977. Simple applications of McWilliams' "A note on a consistent quasigeostrophic model in a multiply connected domain." Dyn. Atm. Oceans, *1,* 443–453.
Groves, G. W. and E. J. Hannan. 1968. Time series regression of sea level on weather. Rev. Geophys., *6,* 129–174.
Groves, G. W. and B. D. Zetler. 1964. The cross spectrum of sea level at San Francisco and Honolulu. J. Mar. Res., *22,* 269–275.
Hendershott, M. C. 1989. Beta-plane Rossby waves over periodic relief. J. Fluid Mech., (submitted).
Hendershott, M. C. and A. J. Miller. 1989. Topographic Rossby waves over a regular lattice of dissimilar seamounts. J. Fluid Mech., (submitted).
Hu, J.-H. and P. P. Niiler. 1987. NEPAC Current Meter and XBT Data for the Circulation in

Northeast Pacific Thermocline 42N and 28N, 152W July 1982. October 1985. Scripps Inst. of Oceanogr. Tech. Rep., SIO Reference No. 87-4.

Jansons, K. M. and E. R. Johnson. 1988. Topographic Rossby waves above a random array of seamountains. J. Fluid Mech., *191,* 373–388.

Larichev, V. 1974. Statement of an internal boundary-value problem for the Rossby-wave equation. (Registration of waves by coastal wave recorders.) Izv. Atmos. Ocean. Phys., *10,* 470–473.

Lawrence, W. and J. Spiesberger. 1989. Measurements of a barotropic planetary vorticity mode in an eddy-resolving quasi-geoseostrophic model using acoustic tomography. J. Phys. Oceanogr., (in press).

Longuet-Higgins, M. S. 1964. Planetary waves on a rotating sphere. Proc. Roy. Soc. A, *279,* 446–473.

—— 1965. Planetary waves on a rotating sphere. II. Proc. Roy. Soc. A, *284,* 40–54.

—— 1966. Planetary waves on a hemisphere bounded by meridians of longitude. Phil. Trans. Roy. Soc. Lond., *A260,* 317–350.

—— 1971. On the spectrum of sea level at Oahu. J. Geophys. Res., *76,* 3517–3522.

Longuet-Higgins, M. S. and G. S. Pond. 1970. The free oscillations of fluid on a hemisphere bounded by meridians of longitude. Phil. Trans. Roy. Soc. Lond., *A266,* 193–223.

Luther, D. S. 1980. Observations of long-period waves in the tropical oceans and atmosphere. Ph.D. dissertation, Joint Program in Oceanography, Massachusetts Institute of Oceanography and the Woods Hole Oceanographic Institution, 210 pp.

—— 1982. Evidence of a 4–6 day barotropic, planetary oscillation of the Pacific Ocean. J. Phys. Oceanogr., *12,* 644–657.

Luther D. S., A. D. Chave and J. H. Filloux. 1987. BEMPEX: A study of barotropic ocean currents and lithospheric electrical conductivity. EOS, *68,* 618–619 and 628–629.

Miller, A. J. 1986a. Non-divergent planetary oscillations in mid-latitude ocean basins with continental shelves. J. Phys. Oceanogr., *16,* 1914–1928.

—— 1986b. Barotropic Planetary-Topographic Oscillations in Ocean Basins. Ph.D. dissertation, Scripps Institution of Oceanography, University of California, San Diego, 133 pp.

Miller, A. J., W. R. Holland and M. C. Hendershott. 1987. Open-ocean response and normal-mode excitation in an eddy-resolving general circulation model. Geophys. Astrophys. Fluid Dyn., *37,* 253–278.

Mofjeld, H. O., and M. Rattray, Jr. 1971. Free oscillations in a β-plane ocean. J. Mar. Res., *29,* 281–305.

Platzman, G. W. 1975. Normal modes of the Atlantic and Indian Oceans. J. Phys. Oceanogr., *11,* 579–603.

—— 1978. Normal modes of the world ocean. Part I. Design of a finite element barotropic model. J. Phys. Oceanogr., *8,* 323–343.

—— 1981. A Guide to FORTRAN Programs for Normal Modes of the Ocean. Vol. I., The University of Chicago. Tech. Rep. to the National Science Foundation, 81 pp.

—— 1985. Normal Modes of the World Ocean: Maps and Tables. The University of Chicago. Tech. Rep. to the National Science Foundation, 97 pp.

Platzman, G. W., G. A. Curtis, K. S. Hansen and R. D. Slater. 1981. Normal modes of the world ocean. Part II. Description of modes in the period range 8–80 hours. J. Phys. Oceanogr., *11,* 579–603.

Rattray, M., Jr. and R. L. Charnell. 1966. Quasigeostrophic free oscillations in enclosed basins. J. Mar. Res., *24,* 82–103.

Rhines, P. B. 1969. Slow oscillations in an ocean of varying depth. Part 1. Abrupt topography. J. Fluid Mech., *37,* 161–189.

Rhines, P. B. and F. P. Bretherton. 1973. Topographic Rossby waves in a rough-bottomed ocean. J. Fluid Mech., *61*, 583–607.

Ripa. P. 1978. Normal Rossby modes of a closed basin with topography. J. Geophys. Res., *83*, 1947–1957.